Human influence reshapes land–sea seasonal temperature rhythms

Wang, A., Duan, J., Fu, S., Dong, B. ORCID: https://orcid.org/0000-0003-0809-7911, Hao, F. and Stott, P. A. (2025) Human influence reshapes land–sea seasonal temperature rhythms. Geophysical Research Letters, 52 (24). e2025GL119736. ISSN 1944-8007 doi: 10.1029/2025GL119736 Available at https://centaur.reading.ac.uk/127661/

Geophysical Research Letters

RESEARCH LETTER
10.1029/2025GL119736

Human Influence Reshapes Land–Sea Seasonal Temperature Rhythms

Anqi Wang[1,2], Jianping Duan[3], Shenming Fu[1], Buwen Dong[4], Fengqi Hao[3], and Peter A. Stott[5]

[1]State Key Laboratory of Earth System Numerical Modeling and Application, Institute of Atmospheric Physics, Chinese Academy of Sciences, Beijing, China, [2]University of Chinese Academy of Sciences, Beijing, China, [3]State Key Laboratory of Earth Surface Processes and Disaster Risk Reduction, Faculty of Geographical Science, Beijing Normal University, Beijing, China, [4]National Centre for Atmospheric Science, Department of Meteorology, University of Reading, Reading, UK, [5]Met Office Hadley Centre, Exeter, UK

Abstract The land–sea thermal contrast is one of the original drivers of the Earth's climate system and has undergone significant changes in the recent period. However, the seasonality and geographic profile of these changes remain unclear. Here, we reveal an anthropogenic-forced seasonal change in the land–sea thermal contrast by analyzing the evolution of its temperature annual cycle ($TAC_{L–S}$). We find a significant reduction in $TAC_{L–S}$ in the northern mid-latitudes, dominated by stronger winter land warming, alongside an increase in the northern high latitudes, dominated by stronger winter sea warming, during 1941–2014. In particular, these anthropogenic changes are projected to intensify in 2015–2100, with an additional emergence of $TAC_{L–S}$ increases dominated by summer land warming in the southern mid-latitudes. Thus, a future tripolar pattern of $TAC_{L–S}$ heralds novel land–sea climate regimes with far-reaching climatic impacts.

Plain Language Summary The land–sea thermal contrast constitutes an important energy source for numerous large-scale atmospheric circulations. While previous studies on the changing land–sea thermal contrast generally focus on single seasons, we here reveal shifts in the land–sea contrast in temperature annual cycle (TAC) amplitude driven by human activity. We find that the land–sea TAC amplitude difference has increased in northern high latitudes but reduced in northern mid-latitudes during the historical period. Future projections suggest that, except for the further intensification of the increased/reduced TAC in the northern high-/mid-latitudes, a significant increase of land–sea TAC amplitude would emerge in the southern mid-latitudes. Our results indicate a human-induced reshaping of land–sea thermal contrast characterized as the zonal TAC increase or reduction.

Key Points:

- Human activity is reshaping land–sea annual temperature cycle amplitude differences ($TAC_{L–S}$)
- Anthropogenic warming reduced $TAC_{L–S}$ in northern mid-latitudes but increased it in northern high latitudes
- An additional increase in $TAC_{L–S}$ is projected to emerge in the southern mid-latitudes

Supporting Information:

Supporting Information may be found in the online version of this article.

Correspondence to:

J. Duan,
duanjp@bnu.edu.cn

Citation:

Wang, A., Duan, J., Fu, S., Dong, B., Hao, F., & Stott, P. A. (2025). Human influence reshapes land–sea seasonal temperature rhythms. *Geophysical Research Letters*, *52*, e2025GL119736. https://doi.org/10.1029/2025GL119736

Received 30 SEP 2025
Accepted 3 DEC 2025

Author Contributions:

Conceptualization: Jianping Duan
Funding acquisition: Jianping Duan
Project administration: Jianping Duan
Supervision: Jianping Duan
Validation: Anqi Wang
Visualization: Anqi Wang
Writing – original draft: Anqi Wang, Jianping Duan
Writing – review & editing: Anqi Wang, Jianping Duan, Shenming Fu, Buwen Dong, Fengqi Hao, Peter A. Stott

1. Introduction

Global climate, particularly near-surface air temperatures (SAT), has undergone substantial changes since industrialization (Calvin et al., 2023). Among these variations, changes in the magnitude of the temperature annual cycle (TAC) have far-reaching implications for human society and the biosphere. Changes in the TAC influence hydropower production, energy demand, raw material availability, and agricultural practices, and also shape the distribution, abundance, and seasonal activities of animals and plants (Cohen et al., 2018; Kwiecien et al., 2022; Parmesan & Yohe, 2003; Root et al., 2005; Santer et al., 2022). Land–sea thermal contrasts drive large-scale atmosphere circulation systems and profoundly influence the global climate system (Wu et al., 2012). However, these contrasts have been reported to change in a seasonally asymmetric manner, increasing in summer and decreasing in winter (He et al., 2018; Yao et al., 2019) in most regions. This seasonal asymmetry is accompanied by uneven seasonal changes in SAT, leading to a significant shift in the TAC amplitude with a widespread weakening over land (Deng & Fu, 2023; Duan et al., 2019; Hu et al., 2022; Stine et al., 2009) and an amplification over oceans (Liu et al., 2024; Shi et al., 2024). Despite this, the seasonal sources and underlying causes of such asymmetry remain incompletely understood.

In addition to seasonal asymmetry, the spatial distribution of these changes is highly heterogeneous. Across China's coastal zone, for instance, the land–sea thermal contrasts decreased with the decrease in latitude both in summer and winter (Yao et al., 2019). Additionally, in the Far East, summer land–sea thermal contrasts are observed to increase markedly compared to surrounding regions (Kamae et al., 2014). Similarly, in the northern mid-latitudes, stronger decrease/increase in TAC amplitude over land/sea compared to lower latitudes also occurred (Duan et al., 2019; Liu et al., 2024). Despite the observed seasonal and spatial variations, the extent to

which land–sea thermal contrasts contribute to changes in the land–sea TAC amplitude ($TAC_{L–S}$) remains poorly understood, especially, as human activities are widely regarded as the dominant driver of many aspects of climate change (Seneviratne et al., 2016), while it is still uncertain whether anthropogenic forcing contributes to the changes in $TAC_{L–S}$.

In this study, we combine observations and global climate model (GCM) simulations derived from the Coupled Model Intercomparison Project Phase 6 (CMIP6; Eyring et al., 2016) to address the evolution of $TAC_{L–S}$ by analyzing the spatiotemporal dynamics of $TAC_{L–S}$ changes throughout the historical (1851–2014) and future (2015–2100) periods at the global scale. Our objectives are to (a) reveal the spatial pattern and seasonal origins of the changing $TAC_{L–S}$ in the historical periods, (b) detect and quantify anthropogenic contributions in the changing $TAC_{L–S}$, and (c) project the future trends in $TAC_{L–S}$. Our study provides a new insight into how the spatiotemporal heterogeneity of SAT changes and anthropogenic forcing shape climate variability and long-term change.

2. Data and Methods

2.1. Observed and Reanalyzed Data

Observed monthly mean surface temperature data sets, including the Met Office Hadley Centre/Climatic Research Unit global surface temperature data set (HadCRUT5, version 5.1.0.0; 5° × 5°; Morice et al., 2021) and the Berkeley Earth Surface Temperature data set (Berkeley Earth; 1° × 1°; Rohde & Hausfather, 2020), were used to map global TAC amplitude back to 1850. HadCRUT5 here refers to the infilled analysis variant with improved spatial completeness. Both data sets are blended land near-surface air temperature (SAT) and sea-surface temperature (SST) anomaly and extend back to 1850. Monthly mean surface temperature reanalyses from the European Centre for Medium-Range Weather Forecasts Reanalysis v5 (ERA5; 1940–2025, 0.25° × 0.25°; Hersbach et al., 2020) were also used in this study. To explore $TAC_{L–S}$ evolution, HadCRUT5 (best consistency with other data sets; Table S1 in Supporting Information S1) and ERA5 (longest reanalysis coverage) were used. All data sets in this study are re-gridded onto a 5° × 5° grid through a bilinear interpolation to ensure a uniform spatial resolution. Changes in spatial resolution and interpolation methods do not affect the main conclusions of this study (Figure S1 in Supporting Information S1). Anomalies for these data sets, including model simulations, are calculated consistently relative to the 1971–2000 climatology.

2.2. Climate Model Simulations

Seven CMIP6 models (Table S2 in Supporting Information S1) that provide required experiments—historical (ALL), hist-aer (anthropogenic aerosols only forcing, AA), hist-GHG (greenhouse gas only forcing, GHG), hist-nat (natural only forcing, NAT), and piControl (pre-industrial control forcing)—with at least three ensemble members for each experiment (excluding piControl, with only one member) are used. The hist-aer GISS-E2-1-G output (1940–1970) shows clear inconsistencies and is deemed unreasonable; thus, this study uses 18 hist-aer members from six models. The anthropogenic forced component (ANT) is assessed by the difference between ALL and NAT simulations. To reduce internal variability and ensure equal weighting for each model, three realizations in each experiment of CMIP6 models (except piControl) are used in the detection and attribution analysis.

Outputs of shared socioeconomic pathway scenario simulations, including SSP1-2.6, SSP2-4.5, SSP3-7.0, and SSP5-8.5 from 27 ensemble members of 9 models (Table S2 in Supporting Information S1) are used in future projections. SSP2-4.5, SSP3-7.0, and SSP5-8.5 represent medium and high radiative forcing by the end of the 21st century, while SSP1-2.6 provides a sustainable pathway (Eyring et al., 2016).

3. Results

3.1. Global Profile of Land–Sea TAC Amplitude

To overcome period-dependent trends, the two longest observation data sets, HadCRUT5 and Berkeley Earth data, spanning from 1850 to 2014, are used to calculate the TAC amplitude (defined as the mean SAT from June to August of the current year minus the mean SAT from December of the previous year to February of the current year in the Northern Hemisphere, with seasons reversed in the Southern Hemisphere; Text S1 in Supporting Information S1) and to reveal the long-term global pattern of changes in $TAC_{L–S}$ (Figure 1). TAC amplitude is

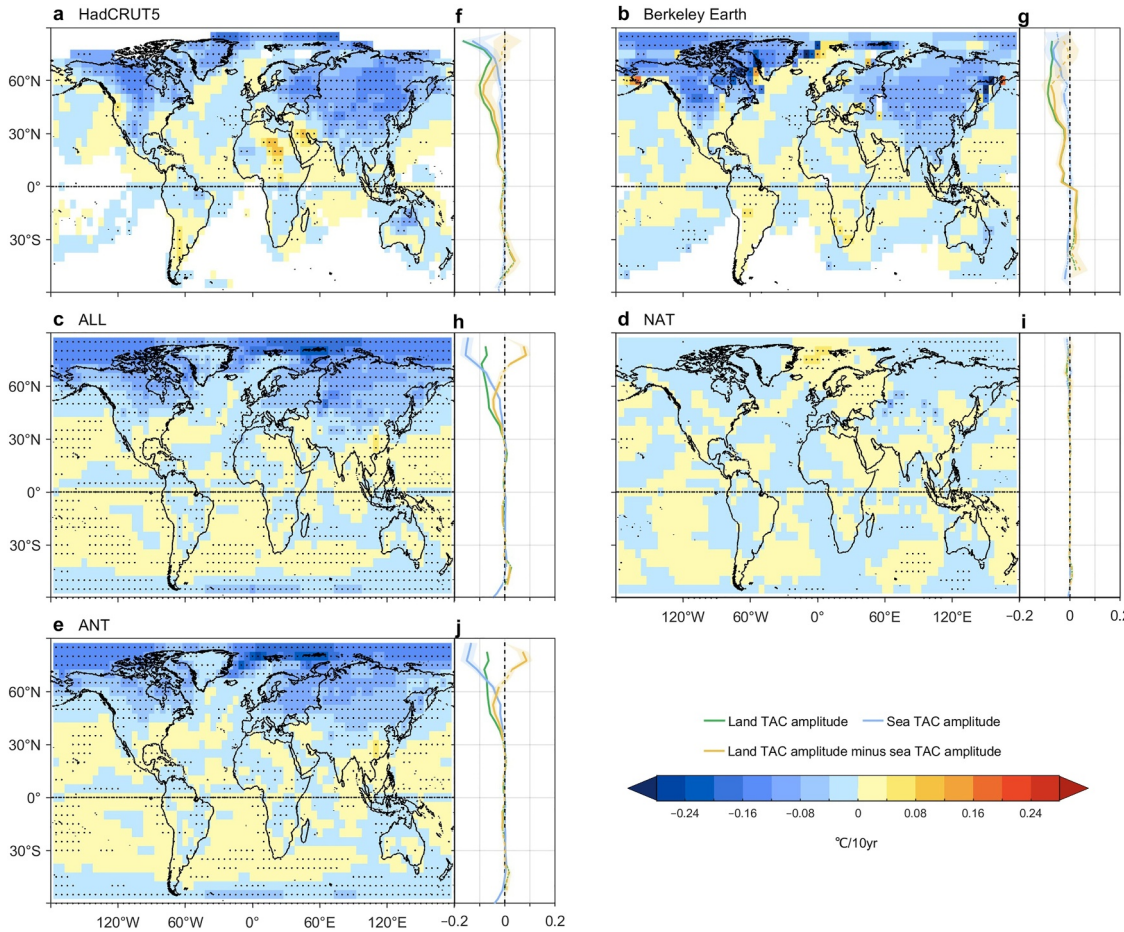

Figure 1. The global profile of trends in the temperature annual cycle (TAC) amplitude anomaly over the longest common interval (i.e., 1851–2014) of observations (a, b) with simulations in ALL (c), NAT (d) and ANT (e) based on the ensemble mean (MME) of GCMs from CMIP6. (f–j), Trends in the zonal mean of TAC amplitude over sea (blue), land (green), and the TAC_{L-S} (yellow) based on HadCRUT5 (f), Berkeley Earth (g), ALL (h), NAT (i) and ANT (j). The shaded areas and the solid/dashed line in panels (f–j) indicate the 5%–95% uncertainty ranges of the trend in the zonal mean of TAC amplitude anomaly, and the trend is significant/non-significant at a level of 0.05, respectively. Stippling in panels (a–e) means the trend in TAC amplitude in the period 1851–2014 is significant at the level of 0.05.

generally larger over land than sea, with the greatest TAC_{L-S} in the northern mid-to-high latitudes and weak values in the low latitudes (30°N–30°S; Figures S2a–S2f in Supporting Information S1). Correspondingly, TAC amplitude trends display a pronounced meridional gradient over both land and sea (Figures 1a and 1b). Trends in TAC amplitude are weak in the low latitudes, while the northern mid-latitudes (30°N–60°N) exhibit a strong decline over land (approximately −0.07°C/10 yr) and a slight decrease over sea (approximately −0.012°C/10 yr; Figures 1f and 1g). In the northern high latitudes, the significant decrease in TAC amplitude occurs both over land (approximately −0.085°C/10 yr) and sea (approximately −0.063°C/10 yr) regions.

Consequently, the trend in TAC_{L-S} also shows a distinct meridional profile (Figures 1f and 1g). The largest reduction of TAC_{L-S} is observed between 30°N and 60°N (approximately −0.056°C/10 yr). The low latitudes and the southern mid-latitudes (30°S–60°S) show a weak trend (less than 0.025°C/10 yr in two data sets).

The ALL-forced multi-model ensemble mean (MME) captures large-scale spatial changes ($r = 0.70$; Table S1 in Supporting Information S1), including the dominant land TAC amplitude decline, the northern mid-latitude TAC_{L-S} reduction, and weak low latitudes changes (Figures 1f–1h). A model–observation discrepancy caused by the SST–SAT difference occurs over northern high-latitude seas, most pronounced in winter and negligible in summer, due to sea ice effects on air–sea energy exchange (Figures S3a–S3f in Supporting Information S1). Meanwhile, observed TAC changes include both internal variability and external forcing induced components, while the ALL-forced MME isolates the forced component (Chen et al., 2019); thus, small-scale discrepancies reflect internal variability, and large-scale agreement indicates a forced response. Consistently, the spatial pattern

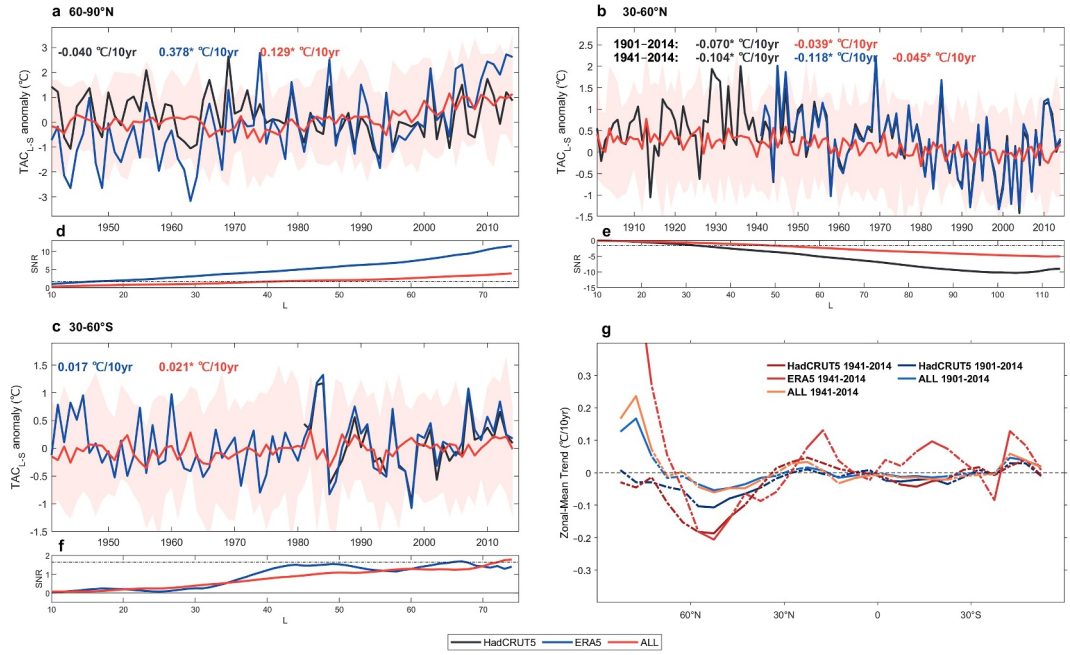

Figure 2. Zonally averaged TAC_{L-S} and the timescale-dependent signal-to-noise ratios (SNR). Panels (a–c), TAC_{L-S} anomaly derived from HadCRUT5 (black solid line), ERA5 (blue solid line), and ALL (red solid line) in the northern high latitudes (a), northern mid-latitudes (b), and southern mid-latitudes (c). Panels (d–f), SNR of TAC_{L-S} based on HadCRUT5, ERA5, and ALL in the northern high latitudes (d), northern mid-latitudes (e), and southern mid-latitudes (f). The dashed line in panels (d, e, f) indicates the threshold for signal emergence. (g) The zonal mean trend of TAC_{L-S} anomaly derived from HadCRUT5, ERA5, and ALL in the periods 1901–2014 and 1941–2014. The solid/dashed line indicates the trend is significant/non-significant at a level of 0.05. The light red shading in panels (a–c) indicates the 5%–95% range of TAC_{L-S} anomaly among individual simulations. Numbers with different colors in panels (a–c) denote the linear trends (°C/10 yr) of TAC_{L-S} anomaly in the period 1901–2014/1941–2014 driven by different data sets, and the asterisk indicates the trend is significant at the level of 0.05.

in ANT closely matches ALL ($r = 0.99$, $p < 0.05$), while NAT shows negligible trends in TAC amplitude and TAC_{L-S} (Figures 1d and 1i), indicating that these changes in TAC in ALL are not due to natural forcing.

3.2. Meridionally Divergent Trends in the Land–Sea TAC Amplitude

Based on the distinct meridional divergences of the TAC_{L-S} (Figures 1f–1h and 2g), we conduct further analysis of trends in the regionally averaged TAC_{L-S} on the northern high latitudes, the northern mid-latitudes and the southern mid-latitudes with multiple data sets during their reliable periods. Given discrepancies in TAC amplitude trends between Berkeley Earth and HadCRUT5 data sets in the northern high latitudes and southern mid-latitudes caused by limited data coverage (Figures 1f and 1g), the well-validated ERA5 (Figures S4a and S4c in Supporting Information S1) data set with complete grid coverage is also included in the further analyses. In the sea regions of the northern high latitude, considering SAT rather than SST is more reasonable for conducting the TAC_{L-S} analysis (detailed descriptions in Text S2 in Supporting Information S1), our analysis mainly relies on ERA5 since 1941 (Figure 2a). Reliable northern mid-latitude TAC_{L-S} estimates are available back to 1901 in HadCRUT5 (Figures S5b and S5e in Supporting Information S1) and to 1941 in ERA5, with strong agreement during 1941–2014 (Figure 2b). Similarly, for the southern mid-latitudes, the analysis is performed using ERA5 (1941–2014) and HadCRUT5 (1981–2014; Figure S5f in Supporting Information S1). Despite the shorter overlap, the two data sets show strong agreement in $TAC_{L-S,}$ enabling reliable long-term assessment.

TAC_{L-S} trends show distinct latitudinal contrasts during 1941–2014 (Figures 2a–2c): significant decreases in the northern mid-latitudes (−0.118°C/10 yr in ERA5; −0.104°C/10 yr in HadCRUT5), a marked increase in the northern high latitudes (0.378°C/10 yr in ERA5), and a weak change in the southern mid-latitudes (0.017°C/10 yr in ERA5), showing good agreement with other observational data sets (Figure S6 in Supporting Information S1). Simulated TAC_{L-S} ranges basically coincide with observed variability and trends across all three latitude bands,

10.1029/2025GL119736

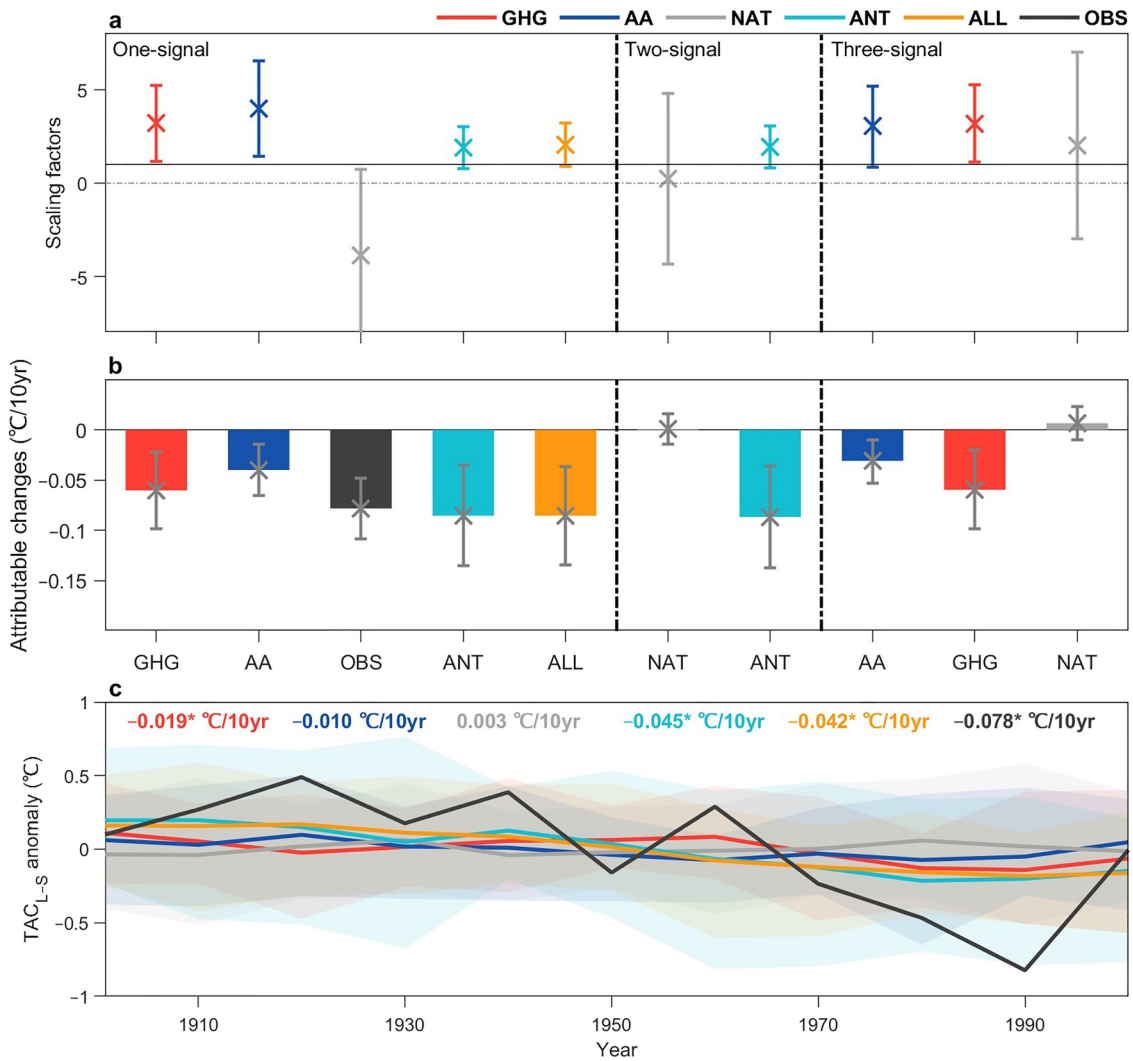

Figure 3. Results of D&A analyses for TAC_{L-S} trends in the 30°–60°N during 1901–2014. (a) Scaling factors and the 90% confidence interval derived from one-signal (left), two-signal (middle), and three-signal (right) analyses. (b) The attributable contributions to different forcings (colored bar) with the 90% confidence interval (black bars) for the one-signal (left), two-signal (middle) and three-signal (right) case. (c) Non-overlapping 10-year-averaged series of TAC_{L-S} anomaly derived from observations and simulations driven by different forcings with the 5%–95% range among individual simulations. Numbers with different colors in panel (c) denote the linear trends (°C/10 yr) of 10-year-averaged TAC_{L-S} anomaly, and the asterisk indicates the trend is significant at the level of 0.05.

though trends are weaker in the northern regions and stronger in the southern regions. The most pronounced changes occur in the northern high latitudes, as shown both in ERA5 and the ALL-forced MME (Figure 2g). Consistent significant decreases in TAC_{L-S} during both 1901–2014 and 1941–2014 reflect a robust long-term trend in the northern mid-latitudes.

Timescale-dependent SNR analysis (Santer et al., 2011; Text S3 in Supporting Information S1) shows that robust TAC_{L-S} signals have emerged (SNR > 1.96) in the northern mid- and high latitudes, but not in the southern mid-latitudes (Figures 2d–2f). Meanwhile, the SNR was always detected earlier and stronger in observations/reanalysis than in ALL-forced MME, likely due to weaker simulated trends, except in the southern mid-latitudes.

3.3. Quantitative Attribution for the Changed Land–Sea TAC

Detection and attribution (D&A) analyses based on HadCRUT5 in one-, two-, and three-signal cases for the reduced TAC_{L-S} in the northern mid-latitudes (1901–2014) reveal a clear distinction between ALL and NAT signals (Figure 3; Text S4 in Supporting Information S1). In the one-signal case, although simulations underestimate the observed TAC_{L-S} reduction, the undetectable (the signal is detectable when the 90% confidence

interval of the scaling factor is above zero) NAT signal is clearly separated from ALL, GHG, AA, and ANT (Figure 3a). Consistently, the attributable (90% confidence interval of the scaling factor is above zero and includes 1) ANT and undetectable NAT occur in the two-signal D&A analysis. In the three-signal case, the AA is attributable, the GHG is detectable with an underestimation, and NAT remains undetectable. Seasonal D&A analyses based on land–sea SAT difference ($SAT_{L–S}$) show that AA contributes only to summer $SAT_{L–S}$, while GHG drives both summer and winter $SAT_{L–S}$ changes (Figure S7 in Supporting Information S1). Thus, anthropogenic forcing—mainly GHG year-round and AA in summer—has driven the significant $TAC_{L–S}$ decline in northern mid-latitudes since 1901.

The observed 10-year-averaged $TAC_{L–S}$ trends (−0.078°C/10 yr) closely match ANT (−0.085°C/10 yr; Figure 3b), with NAT exerting only a slight offset. ALL and ANT show nearly identical contributions (−0.085°C/10 yr), consistent with the similar spatial and meridional patterns in observations, ALL, and ANT (Figure 1). In one-signal analysis, AA and GHG reduce $TAC_{L–S}$ by −0.04 and −0.06°C/10 yr, respectively, while in the three-signal case the AA effect weakens to −0.031°C/10 yr, suggesting an AA–GHG interaction (Ribes & Terray, 2013). Non-overlapping 10-year-averaged trend driven by different forcings further confirms the result (Figure 3c).

3.4. Projected $TAC_{L–S}$ Throughout the 21st Century

Future projections under the constrained SSP2-4.5 scenario (Text S5 in Supporting Information S1) indicate an intensified divergence in land–sea TAC amplitude difference (Figure 4). The constrained MME shows strong spatial consistency with the reference data and yields consistent $TAC_{L–S}$ decline/increase across different reference periods and constraint methods (Figures S4a–S4f in Supporting Information S1). A tripolar pattern intensifying with the increasing emission of greenhouse gases (Figures S8a–S8c in Supporting Information S1) emerges during 2015–2100, with $TAC_{L–S}$ increasing in the northern high and southern mid-latitudes but decreasing in the northern mid-latitudes. In the northern high latitudes, projected $TAC_{L–S}$ trends exceed twice the historical rate under SSP2-4.5 and more than 2.5 times under SSP3-7.0/SSP5-8.5, while even SSP1-2.6 shows an approximately 1.3-fold increase, implying an irreversible shift linked to sea-ice loss (Figure S8 in Supporting Information S1). The $TAC_{L–S}$ in the northern mid-latitudes continues to decline, though heterogeneous land TAC trends partly offset this (Figures S9c–S9e in Supporting Information S1). Specifically, land regions in 180°W–75°E and 30°–50°N (NHM2) show a strong TAC amplitude increase during 2015–2100, consistent with adjacent seas, while other northern mid-latitudes regions (NHM1) remain dominated by land decreases (Figure 4b). $TAC_{L–S}$ remains stable in the northern low latitudes, but shows a slight future decline in the southern low latitudes (Figure 4g). In contrast, despite a weak historical signal, the southern mid-latitudes exhibit a pronounced future increase, exceeding that of the northern mid-latitudes.

Projected TAC amplitude trends under SSP2-4.5 driven by different forcings confirm the dominant role of anthropogenic forcing (Figure S10 in Supporting Information S1). ANT and GHG produce trends comparable to ALL, while NAT shows negligible influence. The opposite AA–GHG effects occurred in 1941–2014 over the Northern Hemisphere disappear in future projections, likely due to declining aerosol concentrations (Samset et al., 2025). Thus, future TAC amplitude and $TAC_{L–S}$ changes remain tightly tied to human activity, especially GHGs.

4. Discussion

Changes in $TAC_{L–S}$ stem from divergent land–sea TAC trends and heterogeneous seasonal $SAT_{L–S}$ trends. While changes in land–sea thermal contrast and their climatic impacts have been widely reported (Endo et al., 2018; Jin et al., 2020; Kitoh & Endo, 2025; Portal et al., 2022), most previous studies have focused on specific seasons or regions. Here, based on the distinct latitudinal $SAT_{L–S}$ trends features (Figure S10 in Supporting Information S1), we analyze origins of the changing $TAC_{L–S}$ through seasonal variations across latitude zones.

Positive $SAT_{L–S}$ trends occur in both summer and winter across all three latitude bands, except for northern high-latitude winters (Figure S10 in Supporting Information S1), reflecting stronger land warming than sea due to heat capacity contrasts and land's higher GHG sensitivity (Sutton et al., 2007). In the northern high latitudes, winter decreases and summer increases in $SAT_{L–S}$ jointly drive a pronounced $TAC_{L–S}$ rise, consistent with ANT- and GHG-driven simulations. The winter decline is inferred to be mainly caused by GHG-driven sea ice loss, which exposes open water and accelerates sea warming relative to land (Chen et al., 2019; Dai et al., 2019). This sea ice–

10.1029/2025GL119736

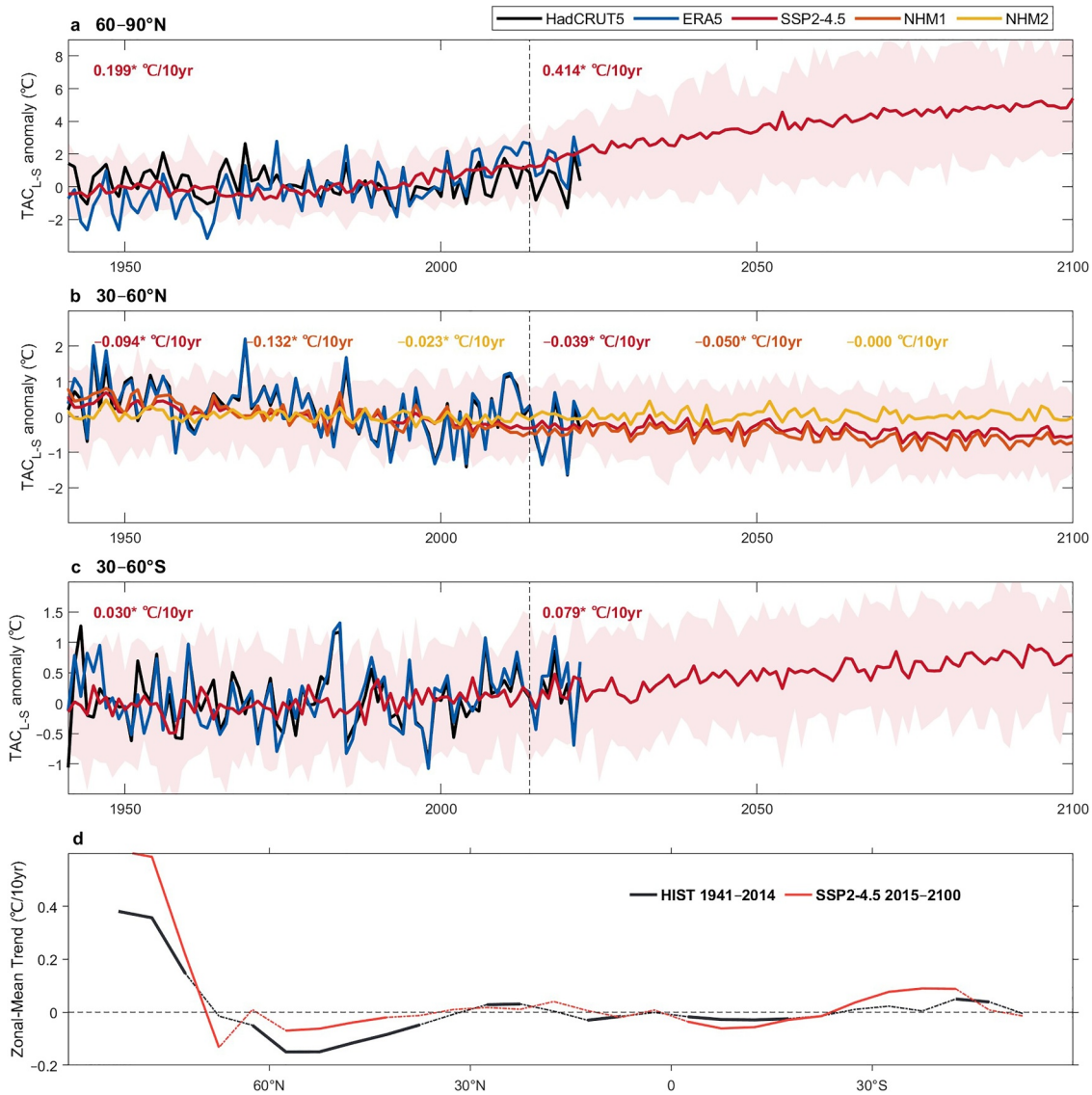

Figure 4. Projected global TAC_{L-S} in the future (2015–2100) and the comparisons of their historical (1941–2014) changes with observations. (a–c) Zonally averaged TAC_{L-S} anomaly over 60°–90°N (a), 30°–60°N (b), 30°–60°S (c) based on ERA5, HadCRUT5, historical simulations, and the constrained SSP2-4.5 scenarios. (d) Zonal mean trend of TAC_{L-S} anomaly driven by historical ALL-forced MME and by SSP2-4.5. The solid/dashed line indicates a significant/non-significant trend at the level of 0.05. Numbers with different colors in panels (a–c) denote the linear trends (°C/10 yr) of TAC_{L-S} in the historical period (left) and future (right). The asterisk denotes significance at the 0.05 level, and the vertical dashed line in panels (a–c) marks 2014.

driven seasonal asymmetry persists in both historical and future periods and remains significant even under SSP1-2.6 (Figures S8a, S8g, and S11a in Supporting Information S1).

Typically, in the northern mid-latitudes, previous studies have reported that the winter land–sea SAT contrast has decreased while the summer contrast has increased (Wu et al., 2022), with a larger change in winter (i.e., a stronger increase in winter SAT_{L-S}) (He et al., 2018). This is consistent with our results driven by the ANT-forced MME (Figure S10b in Supporting Information S1). This seasonal contrast is mainly attributed to (a) slower winter sea warming than summer due to the deeper winter mixed layer with larger heat capacity (Jo et al., 2022), amplifying summer warming under GHG forcing—a mechanism more evident in the future; and (b) stronger winter land warming may contributed by GHG-induced Arctic amplification (Chen et al., 2019; Dai et al., 2019; Hu et al., 2022) in poleward of 50°N (Figure S9c in Supporting Information S1), important in both historical and future periods. Combined, enhanced summer warming over the sea and intensified winter warming over land

yield a larger winter SAT_{L-S} increase, thereby contributing to a decline in TAC_{L-S} (Figure S11b in Supporting Information S1).

In the southern mid-latitudes, stronger summer than winter land warming (0.130 vs. 0.037°C/10 yr) drives a marked future TAC_{L-S} increase (Figure S10c in Supporting Information S1). This amplification also appears in NHM2, marked by a stronger relative humidity (RH) decline and a weaker specific humidity (q) increase in annual-cycle amplitude (defined here as the difference between summer and winter) than adjacent land regions (Figures S12f and S12i in Supporting Information S1). Rising q strengthens the greenhouse effect, while declining RH reduces cloud cover and increases shortwave radiation (Tang et al., 2024), both contributing to surface warming. In NHM2, stronger RH decreases over land than sea occur in both seasons (Figures S12g and S12h in Supporting Information S1), partly enhancing SAT_{L-S}. Beyond this contrast, summer land warming exceeds winter due to stronger insolation amplifying cloud reduction and water-vapor feedback. Simulations consistently show reduced RH and increased TAC and q amplitudes (Figures S12c, S12f, and S12i in Supporting Information S1). Slower growth of q relative to temperature-driven saturation specific humidity (Clausius–Clapeyron relation) in these regions drives a stronger RH decrease, thereby enhancing TAC amplitude.

All changes are primarily associated with ANT, especially the GHG (Figures S10 and S11 in Supporting Information S1). GHG-induced warming drives sea-ice loss in northern high latitudes and increases water vapor over NHM2 and southern mid-latitudes land regions throughout the analysis period. In contrast, AA caused summer cooling and reduced TAC amplitude in northern mid-to-high latitudes historically (Duan et al., 2019), but this effect weakens in future projections with aerosol decline, leaving enhanced GHG and additional summer warming from aerosol abatement (Deng & Fu, 2023; Samset et al., 2018). Consequently, GHG drives continued TAC_{L-S} decline in northern mid-latitudes, with partly offset by aerosol abatement, while both forcings increase TAC_{L-S} in northern high latitudes. Such human-induced meridionally asymmetric changes in TAC_{L-S} suggest latitude-dependent shifts in land–sea thermal interaction and possible modifications to monsoons and horizontal wind shear. The potential impacts on agriculture and ecosystems, and the implications for mitigation and adaptation, also warrant further consideration.

5. Conclusions

Based on analyses of multiple data sets, we show that anthropogenic forcings are reshaping the seasonal land–sea temperature rhythm into a tripolar pattern: increasing TAC_{L-S} in the northern high and southern mid-latitudes, and decreasing TAC_{L-S} in the northern mid-latitudes. Increases in the northern high latitudes stem from a stronger winter sea warming. In the southern mid-latitudes, which showed minimal historical change, the projected pronounced future increase is induced by a stronger summer land warming. In contrast, the northern mid-latitudes exhibit a sustained decline in TAC_{L-S} stemming from stronger winter land warming and summer sea warming, although there is a spatial heterogeneity over land. This tripolar pattern is expected to intensify with continued greenhouse gas emissions.

Changes in land–sea TAC amplitude contrast closely follow changing land–sea thermal contrast, which strengthens in summer across all latitude bands and in winter at northern high latitudes, but weakens in winter at mid-latitudes in both hemispheres throughout history and projections. For example, in the northern mid-latitudes, land–sea thermal contrast strengthens in summer but weakens in winter, potentially intensifying summer circulation and precipitation while weakening them in winter. These findings highlight the growing need for further research on the climate impact brought by the changing TAC_{L-S} and suggest that a reduction in greenhouse gas emissions may help mitigate the amplifying TAC_{L-S}.

Conflict of Interest

The authors declare no conflicts of interest relevant to this study.

Data Availability Statement

All data sets used in this study are publicly available, including the ERA5 (Hersbach et al., 2020) reanalysis data from the European Centre for Medium-Range Weather Forecasts (ECMWF): https://cds.climate.copernicus.eu/datasets/reanalysis-era5-single-levels-monthly-means?tab=overview; Berkeley Earth temperature (Rohde &

Hausfather, 2020): https://berkeleyearth.org/data/; HadCRUT.5.1.0.0 blended land air temperature and sea-surface temperature anomaly data set (Morice et al., 2021): https://crudata.uea.ac.uk/cru/data/temperature/; Model simulation from Coupled Model Intercomparison Project Phase 6 (CMIP6; Eyring et al., 2016): https://aims2.llnl.gov/search/cmip6/.

Acknowledgments
We acknowledge all institutions that provided the GCM outputs and observational data sets used in this study, including the Met Office Hadley Centre/Climatic Research Unit, Berkeley Earth Surface Temperature Project, European Centre for Medium-Range Weather Forecasts, NASA Goddard Institute for Space Studies, Japan Meteorological Agency and NASA Goddard Space Flight Center. We thank the World Climate Research Programme's Working Group on Coupled Modelling and all institutions for designing the individual CMIP6 climate models used in this study (Table S2 in Supporting Information S1). BD is supported by the UK National Centre for Atmospheric Science, funded by the Natural Environment Research Council. Peter Stott was supported by the Met Office Climate Science for Service Partnership (CSSP) China project under the International Science Partnerships Fund (ISPF).

References

Calvin, K., Dasgupta, D., Krinner, G., Mukherji, A., Thorne, P. W., Trisos, C., et al. (2023). IPCC, 2023: Climate change 2023: Synthesis report. In H. Lee & J. Romero (Eds.), *Contribution of working groups I, II and III to the sixth assessment report of the intergovernmental panel on climate change [Core Writing Team]*. Intergovernmental Panel on Climate Change (IPCC). https://doi.org/10.59327/IPCC/AR6-9789291691647

Chen, J., Dai, A., & Zhang, Y. (2019). Projected changes in daily variability and seasonal cycle of near-surface air temperature over the globe during the twenty-first century. *Journal of Climate*, *32*(24), 8537–8561. https://doi.org/10.1175/JCLI-D-19-0438.1

Cohen, J. M., Lajeunesse, M. J., & Rohr, J. R. (2018). A global synthesis of animal phenological responses to climate change. *Nature Climate Change*, *8*(3), 224–228. https://doi.org/10.1038/s41558-018-0067-3

Dai, A., Luo, D., Song, M., & Liu, J. (2019). Arctic amplification is caused by sea-ice loss under increasing CO_2. *Nature Communications*, *10*(1), 121. https://doi.org/10.1038/s41467-018-07954-9

Deng, Q., & Fu, Z. (2023). Regional changes of surface air temperature annual cycle in the Northern Hemisphere land areas. *International Journal of Climatology*, *43*(5), 2238–2249. https://doi.org/10.1002/joc.7972

Duan, J., Ma, Z., Wu, P., Xoplaki, E., Hegerl, G., Li, L., et al. (2019). Detection of human influences on temperature seasonality from the nineteenth century. *Nature Sustainability*, *2*(6), 484–490. https://doi.org/10.1038/s41893-019-0276-4

Endo, H., Kitoh, A., & Ueda, H. (2018). A unique feature of the Asian summer monsoon response to global warming: The role of different land–sea thermal contrast change between the lower and upper troposphere. *SOLA*, *14*, 57–63. https://doi.org/10.2151/sola.2018-010

Eyring, V., Bony, S., Meehl, G. A., Senior, C. A., Stevens, B., Stouffer, R. J., & Taylor, K. E. (2016). Overview of the Coupled Model Intercomparison Project Phase 6 (CMIP6) experimental design and organization [Dataset]. *Geoscientific Model Development*, *9*(5), 1937–1958. https://doi.org/10.5194/gmd-9-1937-2016

He, Y., Huang, J., Li, D., Xie, Y., Zhang, G., Qi, Y., et al. (2018). Comparison of the effect of land-sea thermal contrast on interdecadal variations in winter and summer blockings. *Climate Dynamics*, *51*(4), 1275–1294. https://doi.org/10.1007/s00382-017-3954-9

Hersbach, H., Bell, B., Berrisford, P., Hirahara, S., Horányi, A., Muñoz-Sabater, J., et al. (2020). The ERA5 global reanalysis [Dataset]. *Quarterly Journal of the Royal Meteorological Society*, *146*(730), 1999–2049. https://doi.org/10.1002/qj.3803

Hu, D., Jiang, D., Tian, Z., & Lang, X. (2022). Weakened amplitude and delayed phase of the future temperature seasonal cycle over China during the twenty-first century. *International Journal of Climatology*, *42*(14), 7133–7145. https://doi.org/10.1002/joc.7634

Jin, C., Wang, B., & Liu, J. (2020). Future changes and controlling factors of the eight regional monsoons projected by CMIP6 models. *Journal of Climate*, *33*(21), 9307–9326. https://doi.org/10.1175/JCLI-D-20-0236.1

Jo, A. R., Lee, J., Timmermann, A., Jin, F., Yamaguchi, R., & Gallego, A. (2022). Future amplification of sea surface temperature seasonality due to enhanced ocean stratification. *Geophysical Research Letters*, *49*(9), e2022GL098607. https://doi.org/10.1029/2022GL098607

Kamae, Y., Watanabe, M., Kimoto, M., & Shiogama, H. (2014). Summertime land–sea thermal contrast and atmospheric circulation over East Asia in a warming climate—Part I: Past changes and future projections. *Climate Dynamics*, *43*(9), 2553–2568. https://doi.org/10.1007/s00382-014-2073-0

Kitoh, A., & Endo, H. (2025). The asymmetric response of the spring and autumn atmospheric circulation over East Asia to a warming climate. *Journal of the Meteorological Society of Japan. Series II*, *103*(5), 559–572. https://doi.org/10.2151/jmsj.2025-028

Kwiecien, O., Braun, T., Brunello, C. F., Faulkner, P., Hausmann, N., Helle, G., et al. (2022). What we talk about when we talk about seasonality – A transdisciplinary review. *Earth-Science Reviews*, *225*, 103843. https://doi.org/10.1016/j.earscirev.2021.103843

Liu, F., Song, F., & Luo, Y. (2024). Human-induced intensified seasonal cycle of sea surface temperature. *Nature Communications*, *15*(1), 3948. https://doi.org/10.1038/s41467-024-48381-3

Morice, C. P., Kennedy, J. J., Rayner, N. A., Winn, J. P., Hogan, E., Killick, R. E., et al. (2021). An updated assessment of near-surface temperature change from 1850: The HadCRUT5 data set [Dataset]. *Journal of Geophysical Research: Atmospheres*, *126*(3), e2019JD032361. https://doi.org/10.1029/2019JD032361

Parmesan, C., & Yohe, G. (2003). A globally coherent fingerprint of climate change impacts across natural systems. *Nature*, *421*(6918), 37–42. https://doi.org/10.1038/nature01286

Portal, A., Pasquero, C., D'Andrea, F., Davini, P., Hamouda, M. E., & Rivière, G. (2022). Influence of reduced winter land–sea contrast on the midlatitude atmospheric circulation. *Journal of Climate*, *35*(19), 6237–6251. https://doi.org/10.1175/JCLI-D-21-0941.1

Ribes, A., & Terray, L. (2013). Application of regularised optimal fingerprinting to attribution. Part II: Application to global near-surface temperature. *Climate Dynamics*, *41*(11), 2837–2853. https://doi.org/10.1007/s00382-013-1736-6

Rohde, R. A., & Hausfather, Z. (2020). The Berkeley Earth Land/Ocean temperature record [Dataset]. *Earth System Science Data*, *12*(4), 3469–3479. https://doi.org/10.5194/essd-12-3469-2020

Root, T. L., MacMynowski, D. P., Mastrandrea, M. D., & Schneider, S. H. (2005). Human-modified temperatures induce species changes: Joint attribution. *Proceedings of the National Academy of Sciences*, *102*(21), 7465–7469. https://doi.org/10.1073/pnas.0502286102

Samset, B. H., Sand, M., Smith, C. J., Bauer, S. E., Forster, P. M., Fuglestvedt, J. S., et al. (2018). Climate impacts from a removal of anthropogenic aerosol emissions. *Geophysical Research Letters*, *45*(2), 1020–1029. https://doi.org/10.1002/2017GL076079

Samset, B. H., Wilcox, L. J., Allen, R. J., Stjern, C. W., Lund, M. T., Ahmadi, S., et al. (2025). East Asian aerosol cleanup has likely contributed to the recent acceleration in global warming. *Communications Earth & Environment*, *6*(1), 543. https://doi.org/10.1038/s43247-025-02527-3

Santer, B. D., Mears, C., Doutriaux, C., Caldwell, P., Gleckler, P. J., Wigley, T. M. L., et al. (2011). Separating signal and noise in atmospheric temperature changes: The importance of timescale. *Journal of Geophysical Research*, *116*(D22). https://doi.org/10.1029/2011JD016263

Santer, B. D., Po-Chedley, S., Feldl, N., Fyfe, J. C., Fu, Q., Solomon, S., et al. (2022). Robust anthropogenic signal identified in the seasonal cycle of tropospheric temperature. *Journal of Climate*, *35*(18), 6075–6100. https://doi.org/10.1175/JCLI-D-21-0766.1

Seneviratne, S. I., Donat, M. G., Pitman, A. J., Knutti, R., & Wilby, R. L. (2016). Allowable CO_2 emissions based on regional and impact-related climate targets. *Nature*, *529*(7587), 477–483. https://doi.org/10.1038/nature16542

Shi, J.-R., Santer, B. D., Kwon, Y.-O., & Wijffels, S. E. (2024). The emerging human influence on the seasonal cycle of sea surface temperature. *Nature Climate Change*, *14*(4), 1–9. https://doi.org/10.1038/s41558-024-01958-8

Stine, A. R., Huybers, P., & Fung, I. Y. (2009). Changes in the phase of the annual cycle of surface temperature. *Nature*, *457*(7228), 435–440. https://doi.org/10.1038/nature07675

Sutton, R. T., Dong, B., & Gregory, J. M. (2007). Land/sea warming ratio in response to climate change: IPCC AR4 model results and comparison with observations. *Geophysical Research Letters*, *34*(2). https://doi.org/10.1029/2006GL028164

Tang, T., Lee, X., & Cao, J. (2024). Strengthening of the annual temperature cycle in the mid-latitudes of Northern Hemisphere. *Discover Geoscience*, *2*(1), 96. https://doi.org/10.1007/s44288-024-00098-y

Wu, G., Liu, Y., He, B., Bao, Q., Duan, A., & Jin, F.-F. (2012). Thermal controls on the Asian summer monsoon. *Scientific Reports*, *2*(1), 404. https://doi.org/10.1038/srep00404

Wu, Q.-Y., Li, Q.-Q., Ding, Y.-H., Shen, X.-Y., Zhao, M.-C., & Zhu, Y.-X. (2022). Asian summer monsoon responses to the change of land–sea thermodynamic contrast in a warming climate: CMIP6 projections. *Advances in Climate Change Research*, *13*(2), 205–217. https://doi.org/10.1016/j.accre.2022.01.001

Yao, Y., Zou, X., Zhao, Y., & Wang, T. (2019). Rapid changes in land-sea thermal contrast across China's coastal zone in a warming climate. *Journal of Geophysical Research: Atmospheres*, *124*(4), 2049–2067. https://doi.org/10.1029/2018JD029347

References From the Supporting Information

Ebita, A., Kobayashi, S., Ota, Y., Moriya, M., Kumabe, R., Onogi, K., et al. (2011). The Japanese 55-year reanalysis "JRA-55": An interim report [Dataset]. *Inside Solaris*, *7*, 149–152. https://doi.org/10.2151/sola.2011-038

Gelaro, R., McCarty, W., Suárez, M. J., Todling, R., Molod, A., Takacs, L., et al. (2017). The modern-era retrospective analysis for research and applications, version 2 (MERRA-2) [Dataset]. *Journal of Climate*, *30*(14), 5419–5454. https://doi.org/10.1175/JCLI-D-16-0758.1

Ribes, A., Planton, S., & Terray, L. (2013). Application of regularised optimal fingerprinting to attribution. Part I: Method, properties and idealised analysis. *Climate Dynamics*, *41*(11–12), 2817–2836. https://doi.org/10.1007/s00382-013-1735-7

Tang, H., Wang, J., Chen, Y., Tett, S. F. B., Sun, Y., Cheng, L., et al. (2023). Human contribution to the risk of 2021 Northwestern Pacific concurrent marine and terrestrial summer heat. *Bulletin of the American Meteorological Society*, *104*(3), E673–E679. https://doi.org/10.1175/BAMS-D-22-0238.1

Wang, J., Chen, Y., Liao, W., He, G., Tett, S. F. B., Yan, Z., et al. (2021). Anthropogenic emissions and urbanization increase risk of compound hot extremes in cities. *Nature Climate Change*, *11*(12), 1084–1089. https://doi.org/10.1038/s41558-021-01196-2